Biosensors and Bioelectronics 26 (2010) 1425–1431

Contents lists available at ScienceDirect

Biosensors and Bioelectronics

journal homepage: www.elsevier.com/locate/bios

Long range surface plasmon and hydrogel optical waveguide field-enhanced fluorescence biosensor with 3D hydrogel binding matrix: On the role of diffusion mass transfer

Chun Jen Huang, Jakub Dostalek*, Wolfgang Knoll

Austrian Institute of Technology, Donau-City-Strasse 1, 1220 Vienna, Austria

ARTICLE INFO

Article history:
Received 14 April 2010
Received in revised form 9 July 2010
Accepted 19 July 2010
Available online 19 August 2010

Keywords:
Surface plasmon resonance
Long range surface plasmons
Hydrogel
Hydrogel optical waveguide
Fluorescence
Diffusion

ABSTRACT

An implementation of evanescent wave affinity biosensor with a large-capacity three-dimensional binding matrix for ultra-sensitive detection of molecular analytes is investigated. In the experimental part of the work, highly swollen carboxylated poly(N-isopropylacryamide) (NIPAAm) hydrogel with up to micrometer thickness was grafted to a sensor surface, functionalized with antibody recognition elements and employed for immunoassay-based detection of target molecules contained in a liquid sample. Molecular binding events were detected by long range surface plasmon (LRSP) and hydrogel optical waveguide (HOW) field-enhanced fluorescence spectroscopy. These novel methods allowed probing an extended three-dimensional biointerface with an evanescent field reaching up to several micrometers from the sensor surface. The resonant excitation of LRSP and HOW modes provided strong enhancement of intensity of electromagnetic field that is directly translated into an increased fluorescence signal associated with the binding of fluorophore-labeled molecules. Experimental observations were supported by numerical simulations of mass transfer and affinity binding of target molecules in the hydrogel. Through the optimization of the hydrogel thickness and profile of the probing evanescent wave, low femtomolar limit of detection was achieved.

1. Introduction

Surface plasmon resonance (SPR) biosensors become increasingly popular technology for the detection of chemical and biological analytes (Homola, 2008). In these devices, an analyzed liquid sample with target analyte molecules is brought in contact with a metal sensor surface that is probed by resonantly excited surface plasmons. The capture of analyte molecules by the biomolecular recognition elements immobilized on the surface is optically detected from binding-induced refractive index changes. In order to increase the sensitivity of SPR biosensors, three-dimensional binding matrices composed of polymer materials with highly open structure were employed to accommodate large amounts of bimolecular recognition elements on the surface and to reduce the steric hindrance through linking biomolecules to flexible polymer chains. The carboxymethyl dextran (Lofas and Johnsson, 1990) is an example of the most prominent material that was characterized in great detail and other polymers including different forms of poly(ethylene glycols) were investigated (Andersson et al., 2009; Masson et al., 2004; Tanaka et al., 2009). The thickness of a binding matrix grafted to a SPR biosensor surface is adjusted with respect to the size of target analyte molecules and typically does not exceed 100 nm in order to match the penetration depth of surface plasmon field between 100 and 200 nm. For SPR-based biosensors, these surface architectures allow immobilizing of antibody receptors with surface mass density up to 10 ng mm^{-2} which corresponds to several full packed monolayers (Yu et al., 2004). Only recently, novel SPR-based biosensor detection formats relying on extended evanescent field of long range surface plasmon (LRSP) and hydrogel optical waveguide (HOW) modes for probing crosslinked polymer binding matrices with up to micrometer thickness were developed in our laboratory. These biosensor schemes took advantage of hydrogels based on poly(N-isopropylacryamide) (NIPAAm) and dextran (Beines et al., 2007; Brunsen et al., in preparation) that exhibit large swelling ratio (>10) ensuring fast diffusion of analyte and that can be functionalized by antibodies with surface mass density up to 100 ng mm^{-2} (Wang et al., 2009a) using active ester coupling strategies (Aulasevich et al., 2009). In addition, the responsive properties of hydrogels such as NIPAAm are attractive for further increasing the sensitivity and detection time based on compacting of captured analyte on the surface through a collapse triggered by an external stimulus (Huang et al., 2009). These new schemes were employed in refractometric-based (Wang et al., 2010) and fluorescence spectroscopy-based

* Corresponding author. Fax: +43 50550 4399.
E-mail address: jakub.dostalek@ait.ac.at (J. Dostalek).

0956-5663/$ – see front matter © 2010 Elsevier B.V. All rights reserved.
doi:10.1016/j.bios.2010.07.072

(Wang et al., 2009a) biosensors for detection of protein analytes and were demonstrated to reach the limit of detection at low picomolar and femtomolar levels, respectively.

The effect of diffusion-limited mass transfer of a target analyte to the SPR sensor surface with dextran brush binding matrix was subject to extensive study in order to enable accurate evaluation of biomolecular interaction analysis (BIA) (Edwards, 2001; Schuck, 1996; Sikavitsas et al., 2002). However, to the best of our knowledge the dependence of the sensitivity of SPR-based biosensors for detection of molecular analytes on the diffusion mass transfer to and through an extended large binding capacity hydrogel matrix was not yet investigated in detail. This study addresses design of three-dimensional binding matrices in order to reach ultra-low detection limits and it takes into account the concentration and affinity constants of biomolecular recognition elements, thickness of a hydrogel film, mass transfer of target analyte to and through the hydrogel biointerface as well as the spatial profile of probing evanescent wave. In the experimental part of the work, long range surface plasmon (LRSP) and hydrogel optical waveguide (HOW) field-enhanced fluorescence spectroscopy were used for the detection of fluorophore-labeled analyte molecules captured in a functionalized NIPAAm-based hydrogel binding matrix. Results obtained from an immunoassay experiment were supported by a theoretical model which describes the temporal and spatial evolution of the affinity binding events and analyte diffusion through the functionalized hydrogel film.

2. Materials and methods

2.1. Materials

The synthesis of the NIPAAm-based hydrogel (composed of the terpolymer with N-isoproprylacrylamide, methacrylic acid, and 4-methacryloyl benzophenone), sodium para-tetrafluorophenol-sulfonate (TFPS) and S-3-(benzoylphenoxy)propyl ethanthioate (benzophenone-thiol) was performed at the Max Planck Institute for Polymer Research in Mainz (Germany) as described in the literature (Beines et al., 2007). Mouse immunoglobulin G (IgG) and goat anti-mouse immunoglobulin G (a-IgG) were purchased from Invitrogen (Camarillo, CA). 1-Ethyl-3-(3-dimethylaminopropyl)carbodiimide (EDC) and N-hydroxysulfosuccinimide (NHS) were obtained from Pierce (Rockford, IL). A-IgG molecules were labeled with Alexa Fluor 647 and the dye-to-protein molar ratio was of 4.9 determined by UV spectrometry. Sodium acetate, acetic acid and Tween 20 were purchased from Sigma–Aldrich (Schnelldorf, Germany) and phosphate buffered saline (PBS, 140 mM NaCl, 10 mM phosphate, 3 mM KCl, and a pH of 7.4) was acquired from Calbiochem (Darmstadt, Germany). For the affinity binding experiments, samples were prepared by spiking PBS containing 0.05% Tween 20 (PBST) with a-IgG. For the immobilization of IgG into the hydrogel, IgG was dissolved in 10 mM acetate buffer (ACT with pH 4) that was prepared from sodium acetate by adjusting the pH with acetic acid. Cytop fluoropolymer (CTL-809 M, 9 wt.% in the solvent of CT-solv 180) was obtained from Asahi Glass (Tokyo, Japan).

2.2. Preparation of the layer structure on the sensor surface

The preparation of LRSP-supporting layer structure and the grafting of a NIPAAm-based hydrogel on its surface was performed as described in our previous studies (Huang et al., 2010) and (Aulasevich et al., 2009), respectively. Cytop layer with the thickness of $d_b = 715$ nm was prepared on a glass substrate using spin-coating followed by a deposition of gold thin film with the thickness of $d_m = 13.2$ nm using magnetron sputtering (UNIVEX 450C from Leybold Systems, Germany). Afterwards, the substrate was soaked overnight in a solution of benzophenone-terminated thiol (dissolved at a concentration of 1 mM in absolute ethanol that was purged with argon) in order to form a self-assembled monolayer (SAM). The modified gold surface was rinsed with absolute ethanol, dried in the stream of nitrogen and a thin NIPAAm-based polymer was deposited on its top using spin-coating. A rotating speed of 2000 rpm was applied for 120 s and the thickness of the NIPAAm-based film was controlled by adjusting the concentration of the polymer (between 1 and 20 mg mL^{-1} in ethanol). Finally, the NIPAAm-based hydrogel was dried in a vacuum oven at 50 °C followed by its simultaneous crosslinking and attachment to the gold surface via benzophenone groups by exposing to UV light (with an irradiation dose of 2 J cm^{-2} at a wavelength of $\lambda = 365$ nm). The thickness of dry NIPAAm-based films was determined by a surface profiler (Alpha-Step IQ, KLA Tencor, CA).

2.3. Optical setup

An optical setup based on the angular spectroscopy of guided waves was employed in this study. As shown in Fig. 1a, a monochromatic TM polarized light beam from He–Ne laser (PL610P, Polytec, Germany, power 2 mW, wavelength $\lambda = 632.8$ nm) was coupled

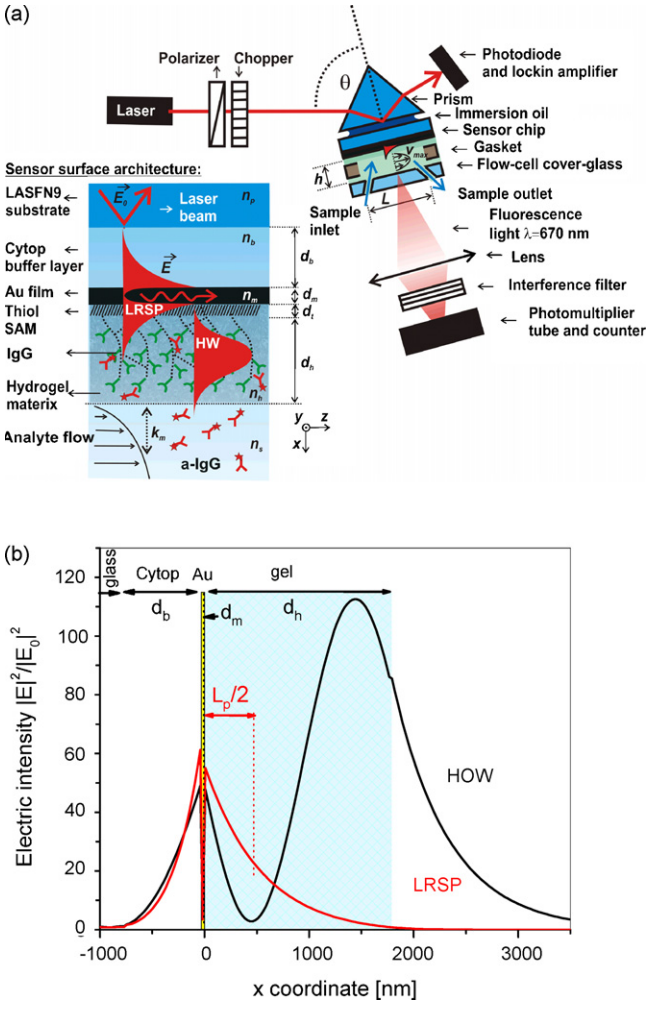

Fig. 1. (a) Setup for the angular spectroscopy of LRSP and HOW modes with a fluorescence spectroscopy module and a scheme of LRSP-supporting layer structure with NIPAAm-based hydrogel binding matrix. (b) Simulated electric intensity profile upon the resonant excitation of LRSP (at the angle of incidence of θ_{LRSP}) and HOW (at the angle of incidence of θ_{HOW}) modes in the hydrogel with a thickness of $d_h = 1.8$ μm and the refractive index of $n_h = 1.345$.

to a 90° LASFN9 optical prism. A glass substrate coated with LRSP-supporting layers and the NIPAAm-based hydrogel film was optically matched to the prism base using refractive index matching oil (Cargille, USA). To the sensor surface, there was attached a flow-cell composed of a poly(dimethylsiloxane) gasket and a transparent quartz slide with input and output ports. The depth of the flow-cell was $h = 0.3$ mm, length $L = 8$ mm and width $w = 5$ mm. The flow-cell input and output ports were connected to a peristaltic pump (Reglo, Ismatec, Switzerland) with a rubber tubing (Tygon R3607, Ismatec, Switzerland) to flow liquid samples at the flow rate of 500 μL min^{-1}. The assembly of prism and flow-cell was mounted on a rotation stage (precision 10^{-3} deg, from Hans Huber AG, Germany) to control the angle of incidence θ and the intensity of the light beam reflected at the prism base was detected using a photodiode and a lock-in amplifier (Model 5210, Princeton Applied Research, USA). As simulations in Fig. 1b show, the resonant coupling to LRSP and HOW modes propagating along the sensor surface are accompanied with enhanced electromagnetic field intensity. This field intensity enhancement provided means for efficient excitation of Alexa Fluor-647 chromophores (absorption wavelength close to 633 nm) in vicinity to the surface. Upon the excitation of LRSPs, the electric field intensity exponentially decays into the hydrogel with the penetration depth of $L_p/2 = 460$ nm. The maximum field intensity enhancement of $|E/E_0|^2 = 55$ occurs at the interface between gold and gel (the electric intensity E was normalized with the intensity of incident light beam E_0). The coupling to HOW provides higher field enhancement of $|E/E_0|^2 = 110$ at a distance of 1400 nm from the gold surface. The fluorescence light emitted by a chromophore Alexa Fluor-647 (emission wavelength of 670 nm) in the gel was collected through the flow-cell using a lens (NA of about 0.3), passed through an interference filter (670FS10-25, L.O.T.-Oriel, Germany) in order to suppress the background and its intensity was measured by a photomultiplier (H6240-01, Hamamatsu, Japan) that was connected to a counter (53131A, Agilent, USA). If the fluorescence signal F exceeded the 10^6 counts per second (cps), attenuation filters were used in order to operate the photomultiplier in the linear regime. By changing the angle of incidence of the laser beam θ, the angular reflectivity $R(\theta)$ and fluorescence $F(\theta)$ spectra were recorded. In vicinity to the critical angle and resonance angles, the scanning step was set below 0.02°. For time dependent measurements of the fluorescence signal $F(t)$, the angle of incidence θ was fixed at the resonance angle for the excitation of LRSP θ_{LRSP} or HOW θ_{HOW} modes providing strong enhancement of the field intensity (see Fig. 1b). The whole optical setup was controlled using the software Wasplas developed at the Max-Planck Institute for Polymer Research in Mainz, Germany.

2.4. Characterization of hydrogel films

The refractive index n_h and the thickness d_h of swollen hydrogel films and refractive index $n_{h\text{-dry}}$ and thickness $d_{h\text{-dry}}$ of dry hydrogel films were determined by the spectroscopy of LRSP and HOW modes as described in our previous reports (Aulasevich et al., 2009; Wang et al., 2009b). For gels with sufficiently large thickness, two resonance dips due to the excitation of LRSP and HOW modes can be observed in the angular reflectivity spectrum $R(\theta)$ centered at distinct angles of θ_{LRSP} and θ_{HOW}, respectively. Due to different profiles of electromagnetic field of LRSP and HOW modes (see Fig. 1b), hydrogel thickness d_h and refractive index n_h can be independently determined by the analysis of reflectivity spectrum $R(\theta)$. The measured reflectivity spectra $R(\theta)$ were fitted by a model based on Fresnel equations and transfer matrix formalism (Yeh, 1998) that was implemented in the software Winspall (developed at the Max Planck Institute for Polymer Research in Mainz, Germany). All parameters of the layer structure except n_h and d_h were fixed at values that were determined by other methods or taken from literature (Hale and Querry, 1973; Huang et al., 2010). These include the refractive index of the LASFN9 glass $n_p = 1.845$, the thickness $d_b = 715$ nm and refractive index $n_b = 1.337$ of Cytop layer, the thickness $d_m = 13.2$ nm and refractive index $n_m = 0.269 + 2.58i$ of gold film, the thickness $d_t = 2$ nm and refractive index $n_t = 1.5$ of benzophenone-thiol SAM and the refractive index of buffer $n_s = 1.333$. In the fitting of angular reflectivity spectra $R(\theta)$, we assumed that the hydrogel refractive index n_h is constant perpendicular to the surface ("box model"). The gel surface mass density was calculated as $\Gamma = (n_h - n_b)d_h\partial c/\partial n_h$, where the factor of $\partial n_h/\partial c = 0.185$ mm^3 mg^{-1} was used (Perlmann and Longsworth, 1948). Based on the effective medium theory, the polymer volume fraction f of the swollen hydrogel was determined as:

$$f = \frac{\left(n_h^2 - n_s^2\right)}{\left(n_h^2 + 2n_s^2\right)} \frac{\left(n_{h\text{-dry}}^2 + 2n_s^2\right)}{\left(n_{h\text{-dry}}^2 - n_s^2\right)} \quad (1)$$

2.5. Modification of the hydrogel film

IgG molecules were *in situ* covalently immobilized to the NIPAAm-based hydrogel matrix via its carboxylic moieties using a protocol developed previously in our group (Aulasevich et al., 2009). Firstly, the hydrogel was swollen in ACT buffer at pH 4 followed by 20 min flow of a mixture of TFPS and EDC (dissolved at concentrations of 21 and 75 mg mL^{-1}, respectively, in water) in order to form terminal TFPS ester moieties. Then, the surface was rinsed with ACT buffer for 3 min and a solution containing IgG molecules at a concentration of 0.64 μM was flowed through the flow-cell for 90 min. After the diffusion of IgG molecules into the gel and their reaction with activated carboxylic groups, the gel was subsequently washed with ACT buffer for 10 min, incubated for 20 min in 1 M ethanolamine solution at pH 8.5 in order to block unreacted TFPS ester groups and then rinsed with the ACT buffer for 15 min. Finally, PBST was flowed over the sensor surface until a stable reflectivity scan $R(\theta)$ was measured.

2.6. Modeling of diffusion and affinity binding in the hydrogel matrix

A numerical model was adopted for the simulation of affinity binding of analyte and diffusion mass transfer based on the theory which was introduced to SPR biosensors with dextran binding matrix (Schuck, 1996). We assumed that biomolecular recognition elements are distributed homogenously in the gel with a concentration β and their interaction with analyte molecules was described by the association and dissociation affinity rate constants k_a and k_d, respectively. A set of partial differential equations describing the mass transfer of analyte from a liquid sample (flowed in a flow-cell) to the hydrogel surface, diffusion of analyte through the hydrogel and its affinity binding to biomolecular recognition elements was numerically solved as described in the Supplemental information. By this model, we calculated the temporal and spatial dependence of the concentration of free $\alpha(x,t)$ and captured $\gamma(x,t)$ analyte in the gel (where x axis is perpendicular to the surface, see Cartesian coordinates in Fig. 1a). Laminar flow of a sample through the flow-cell was assumed and the dependence of the concentration of free α and captured γ analyte on y and z axes (parallel to the sensor surface) was neglected. These approximations are valid as Reynolds and Peclét numbers were equal to Re = 28 and Pe = 3100, respectively. Mass transfer of analyte molecules to the sensor surface was taken into account using two compartment model (Edwards, 2001). The diffusion rate k_m of analyte molecules from an aqueous sample flowed through the flow-cell to the sensor surface was described

as:

$$k_m = 1.378\left(\frac{\nu_{max}{D_s}^2}{hL}\right)^{1/3} \quad (2)$$

where D_s is the diffusion coefficient in the bulk solution and $\nu_{max} = 1.5\upsilon/(hw)$ is the flow velocity in the center of the flow-cell. For the used volumetric flow rate υ, flow-cell geometry (specified in Section 2.3) and the diffusion constant of IgG molecules in aqueous environment of $D_s = 3 \times 10^{-5}$ mm^2 s^{-1} (Jossang et al., 1988), the analyte molecules diffuse to the sensor surface with the diffusion rate of $k_m = 2 \times 10^{-3}$ mm s^{-1}. The simulated sensor signal F_{sim} corresponding to the intensity of the fluorescence light F was assumed to be proportional to the overlap between the concentration of captured molecules $\gamma(x,t)$ and the profile of the field intensity $|E(x)|^2$ of LRSP or HOW modes:

$$F_{sim} \propto \int_0^{d_h} \left|\frac{E(x)}{E_0}\right|^2 \gamma(x,t)\,dx \quad (3)$$

Fluorescence quenching due to the Förster energy transfer in the close proximity to the metal surface was omitted in the model as the hydrogel thickness d_h was typically much larger than the distances up to ~15 nm for which the quenching occurs. In addition, the angular distribution of fluorescence emission that is altered through the interaction of fluorophores with the surface waves (Vasilev et al., 2004) was not taken into account.

3. Results and discussion

3.1. Characteristics of hydrogel films

LRSP-supporting substrates were coated by NIPAAm-based hydrogel layer with a thickness between $d_{h\text{-}dry} = 8$ and 200 nm in the dry state. These gels were swollen in PBST buffer and characterized *in situ* by the spectroscopy of LRSP and HOW modes. Fig. 2a shows the angular reflectivity spectra $R(\theta)$ measured for the hydrogel films with a thickness of $d_{h\text{-}dry} = 0$, 7.4, 82 and 198 nm. The measured reflectivity curves were fitted by Fresnel reflectivity-based model in order to determine hydrogel thickness d_h and refractive index n_h in swollen state. For thicknesses $d_{h\text{-}dry} > 100$ nm, two resonance dips can be observed due to the excitation of LRSP and HOW modes in the swollen gel. Owing to the different profiles of electromagnetic field of LRSP and HOW modes (see Fig. 1b), both n_h and d_h can be determined for these films. For the thickness $d_{h\text{-}dry} < 100$ nm, the swollen hydrogel film does not support HOW and therefore only one of these two parameters can be determined. For such thin gel films, the refractive index n_h was fixed at the value determined for the thicker films and thickness d_h was determined by fitting the LRSP reflectivity dip in the spectrum $R(\theta)$. The obtained results revealed that the thickness of the gel increased after its swelling by a factor of $d_h/d_{h\text{-}dry} = 10.2 \pm 1$ (standard deviation – SD). The refractive index of the hydrogel film changed upon the swelling in PBST from $n_{h\text{-}dry} = 1.503$ in the dry state (see Fig. S2 in Supplemental information) to $n_h = 1.345 \pm 0.002$ (SD) in the swollen state. This change corresponds to the polymer content in the swollen gel of $f = 7.3 \pm 2.4\%$ (SD).

Prior to the affinity binding studies, hydrogel films were modified with IgG molecules using the protocol described in Section 2.5. Fig. 2b shows measured angular reflectivity spectra $R(\theta)$ for a gel with the thickness $d_h = 1800$ nm before and after the immobilization of IgG. One can see that the LRSP dip shifted from $\theta_{LRSP} = 48.67^\circ$ to 48.95° and HOW mode dip moved from $\theta_{HOW} = 47.63^\circ$ to 47.60°. The fitting of reflectivity spectra revealed that the gel surface mass density Γ increased by 15 ± 4% (SD) due to the coupling of IgG. In addition, gel thickness d_h decreased by 20 ± 2% (SD) which is probably due to a lower charge density associated with the converting of negatively charged carboxylic moieties to IgG and neutral ethanolamine groups. The concentration of IgG catcher molecules in the hydrogel β was determined as the increase of the surface mass density Γ divided by the thickness of the gel d_h. The IgG concentration in the gel of $\beta = 16 \pm 4$ mg mL^{-1} (SD) was obtained which corresponds to $\beta = 9 \times 10^{-4} \pm 2.4 \times 10^{-4}$ M for the molecular weight of IgG of 160 kDa. Let us note that for the hydrogel in swollen state with $d_h = 1440$ nm, the surface mass density of the immobilized IgG was 16 ng mm^{-2} which corresponds to about four densely packed monolayers (based on the surface mass density of 4 ng mm^{-2} per monolayer reported by Voellenkle et al. (2004)).

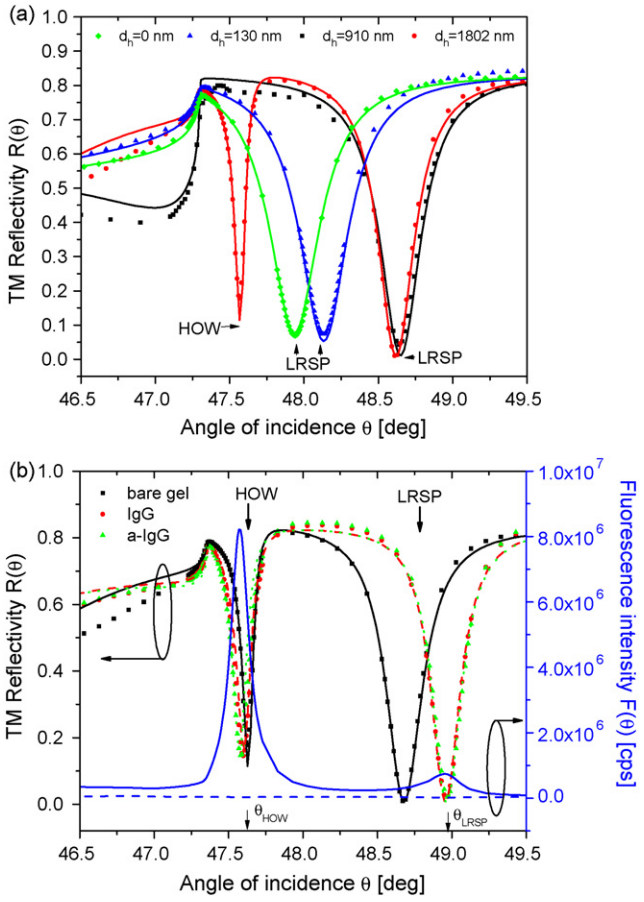

Fig. 2. (a) Angular reflectivity spectra $R(\theta)$ measured for hydrogel films swollen in PBST with the thickness of $d_h = 0$ nm (♦), 160 (▲), 910 nm (■), and 1800 nm (●) and refractive index $n_h = 1.345$ as determined by fitting with a Fresnel equations-based model (lines). (b) Angular reflectivity spectra $R(\theta)$ for hydrogel with the thickness $d_h = 1800$ nm (■) that is swollen in PBST, after its modification with IgG (●) and after the affinity binding of a-IgG labeled with Alexa Fluor-647 (▲) flowed at the concentration of $\alpha_0 = 6.7$ nM for $\Delta t = 30$ min. The measured reflectivity curves were fitted with Fresnel equations-based model (lines). Fluorescence angular spectrum $F(\theta)$ before (dotted line) and after (solid line) the capture of a-IgG labeled with Alexa Fluor 647.

3.2. Kinetics of affinity binding in the hydrogel matrix

LRSP and HOW evanescent waves were excited in order to probe the affinity binding of a-IgG contained in a liquid sample to IgG molecules immobilized in the NIPAAm-based gel. The dependence of the intensity of the binding-induced fluorescence signal F on (a) the hydrogel thickness d_h and (b) on the spatial profile of the probing evanescent wave was investigated. LRSPs with the maximum field intensity at the inner interface of the hydrogel were employed for the observation of hydrogel binding matrices with a

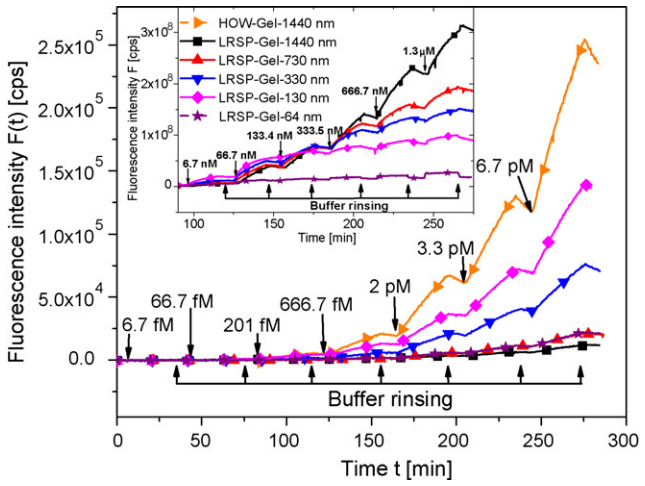

Fig. 3. The binding kinetics observed from the fluorescence signal $F(t)$ that was measured upon the successive flow of samples with a-IgG molecules (labeled with Alexa Fluor-647) at concentrations increasing from $\alpha_0 = 6.7$ fM to 1.3 μM. IgG-functionalized hydrogel binding matrices with the thickness of $d_h = 64$ (×), 130 (♦), 330 (●), 730 (▲) and 1440 nm (■) were probed by LRSP mode and the hydrogel binding matrix with the thickness of $d_h = 1440$ nm was probed by HOW mode (►). Injection times for each sample with a-IgG molecules and rinsing of the sensor surface with buffer are clearly indicated.

thickness between $d_h = 64$ and 1440 nm (measured after the coupling of IgG). HOW mode exhibits the maximum field strength close to the outer hydrogel interface and it was employed for the study of the hydrogel matrix with a thickness of $d_h = 1440$ nm which was sufficiently large to support this mode. The capture of a-IgG analyte molecules labeled with Alexa Fluor 647 chromophores is manifested as an increase in the fluorescence intensity F. Fig. 2b illustrates that after the capture of a-IgG molecules in the gel with the thickness of $d_h = 1400$ nm, the angular fluorescence spectrum $F(\theta)$ exhibits two strong fluorescence peaks located at the angles $\theta_{LRSP} = 48.95^\circ$ and $\theta_{HOW} = 47.60^\circ$ at which the LRSP and HOW modes are excited, respectively.

The fluorescence sensor signal $F(t)$ was measured upon a successive flow of series of samples with increasing concentration of a-IgG α_0. After a baseline was established, each sample was flowed for $\Delta t = 30$ min across the hydrogel surface followed by 10 min rinsing with PBST buffer. As Fig. 3 shows, the affinity binding of a-IgG molecules into the gel is manifested as a gradual increase in the fluorescence signal F. During the rinsing with PBST, a decrease of the signal F occurs due to the dissociation of a-IgG and IgG pairs. For low analyte concentrations α_0 between 6.7 fM and 6.7 pM, the fluorescence signal $F(t)$ linearly increases in time with the slope dF/dt that is proportional to the concentration α_0. For the concentrations α_0 between 6.7 nM and 1.3 μM (see the inset of Fig. 3), the fluorescence signal $F(t)$ become saturated for the hydrogel matrices with $d_h < 1$ μm.

For the probing with LRSP, the fluorescence light intensities F measured after the binding of a-IgG molecules from a sample with high ($\alpha_0 = 1.3$ μM) and low ($\alpha_0 = 0.67$ pM) concentrations of a-IgG were compared with simulations. In these simulations, we used association and dissociation rate constants determined as $k_a = 6.48 \times 10^4 \pm 0.05 \times 10^4\ M^{-1}\ s^{-1}$ and $k_d = 4.46 \times 10^{-5} \pm 0.03 \times 10^{-5}\ s^{-1}$ for the IgG and a-IgG pair as described in the Supplemental information. From data presented in Fig. 4a follows that after the binding of analyte from a sample with large concentration $\alpha_0 = 1.3$ μM the measured fluorescence intensity F increases with the hydrogel thickness d_h. The simulation curves exhibit a similar trend and reach a plateau for a thickness larger than the penetration depth $L_p/2 = 460$ nm. The simulated curves depend weakly on the analyte diffusion coefficient in the gel between $D_g = 3 \times 10^{-7}$ and $3 \times 10^{-5}\ mm^2\ s^{-1}$. For of about six orders of magnitude lower analyte concentration $\alpha_0 = 0.67$ pM, the measured fluorescence signal F is approximately five orders of magnitude smaller and its thickness dependence exhibits different behavior, see Fig. 4b. A maximum fluorescence signal F was measured for the hydrogel thickness between $d_h = 130$ and 410 nm and it sharply decreases when increasing the thickness above these values. The hydrogel thickness for which the simulations predict the maximum fluorescence signal is shifting with the diffusion coefficient in the gel from $d_h = 300$ nm for $D_g = 3 \times 10^{-7}\ mm^2\ s^{-1}$ to $d_h = 580$ nm for $D_g = 3 \times 10^{-5}\ mm^2\ s^{-1}$. The comparison of experimental dependence of fluorescence signal F on the hydrogel thickness d_h presented in Fig. 4b indicates that the diffusion coefficient of a-IgG molecules in the gel D_g was more than order of magnitude lower than that in the aqueous sample D_s. This observation agrees with the results obtained by fluorescence correlation spectroscopy for proteins diffusing to NIPAAm-based hydrogel (Raccis, personal communication).

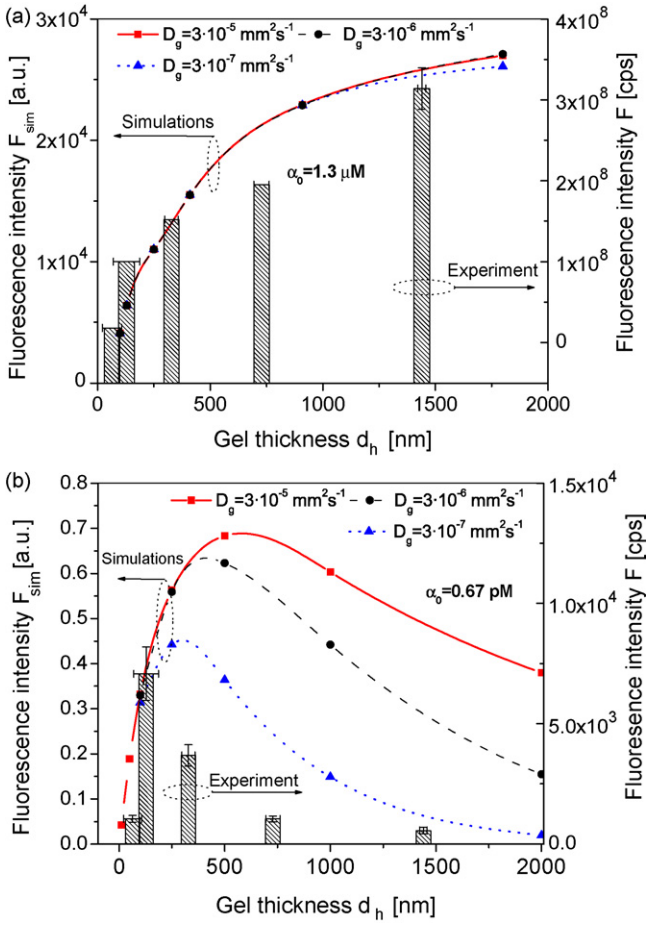

Fig. 4. The comparison of simulated (left axis) and measured (right axis) dependence of the fluorescence signal F on thickness of the hydrogel binding matrix d_h. The hydrogel matrix was probed by LRSP mode the fluorescence signal after the 30 min flow of a-IgG dissolved at (a) low concentration of $\alpha_0 = 0.67$ pM and (b) high concentration of $\alpha_0 = 1.3$ μM. Diffusion coefficient in the gel of $D_g = 3 \times 10^{-5}\ mm^2\ s^{-1}$ (black, ■), $D_g = 3 \times 10^{-6}\ mm^2\ s^{-1}$ (red, ●) and $D_g = 3 \times 10^{-7}\ mm^2\ s^{-1}$ (blue, ▲) was assumed. The errors bar of measured fluorescence signal F represents standard deviation obtained from a triplicate measurement (three prepared sensor chips). (For interpretation of the references to color in this figure legend, the reader is referred to the web version of the article.)

The probing of a-IgG binding by HOW mode provided higher fluorescence signal F than that using LRSPs. Compared to LRSP excitation in the hydrogel with a thickness of $d_h = 130$ nm,

1.8-fold higher fluorescence signal was observed for excitation of HOW in the gel with a thickness of $d_h = 1440$ nm. For LRSP field-enhanced fluorescence spectroscopy, noise of the fluorescence signal baseline $\sigma(F) = 55$ cps (SD) and the maximum slope $dF/(dt\alpha_0) = 0.34$ cps min^{-1} fM^{-1} were measured. For HOW field-enhanced fluorescence spectroscopy, higher noise of the fluorescence signal baseline $\sigma(F) = 107$ cps (SD) and larger slope of $dF/(dt{\cdot}\alpha_0) = 0.59$ cps min^{-1} fM^{-1} were observed. These data correspond to the similar limit of detection below 20 fM determined as $3\sigma(F)/[\Delta t{\cdot}dF/(dt{\cdot}\alpha_0)]$ for both LRSP and HOW-based excitation and hydrogel thicknesses of $d_h = 130$ and 1440 nm, respectively

3.3. The spatial distribution of captured analyte

In order to elucidate the observations presented in Section 3.2, the spatial distribution of captured analyte $\gamma(x)$ was calculated using a numerical model. The simulations predict that after a 30 min flow of a sample with large concentration of $\alpha_0 = 1.3$ μM, the hydrogel binding matrix becomes saturated and $\gamma \sim \beta$ in the whole gel. Therefore, the fluorescence signal F depends weakly on the diffusion of the analyte through the gel and it increases with the number of biomolecular recognition elements within the LRSP evanescent field. The maximum fluorescence signal is achieved for thicknesses d_h that exceeds the LRSP penetration depth $L_p/2 = 460$ nm.

For the analyte concentrations α_0 below pM level, the simulations reveal that concentration of the captured analyte is much smaller than that of biomolecular recognition elements $\gamma \ll \beta$. In such gel, the analyte molecules diffusing from a sample into the gel become captured within a characteristic time t_a and thus can diffuse only to a limited distance from the outer gel interface. The average diffusion time can be shown to be $t_a = \ln(2)/(k_a\beta)$ which corresponds to the following diffusion depth d_p derived using Fick's law:

$$d_p = \sqrt{\frac{4D_g \ln(2)}{k_a\beta}} \quad (4)$$

The numerical simulations shown in Fig. 5 confirm that the binding events preferably occur within an outer hydrogel slice with the thickness d_p. For example, the diffusion penetration depth reaches $d_p = 380$ nm for the diffusion coefficient of $D_g = 3 \times 10^{-7}$ mm^2 s^{-1} and increases to $d_p = 1.2$ μm for $D_g = 3 \times 10^{-6}$ mm^2 s^{-1}. These data illustrate that a more homogenous distribution of $\gamma(x)$ is established in gel with small thickness d_h or for large diffusion coefficients D_g. Let us note that as far as $\gamma \ll \beta$, the established profile of captured analyte does not change in time and the amount of bound analyte is proportional to the flow time $\gamma(x, t) \propto \gamma(x)\Delta t\alpha_0$.

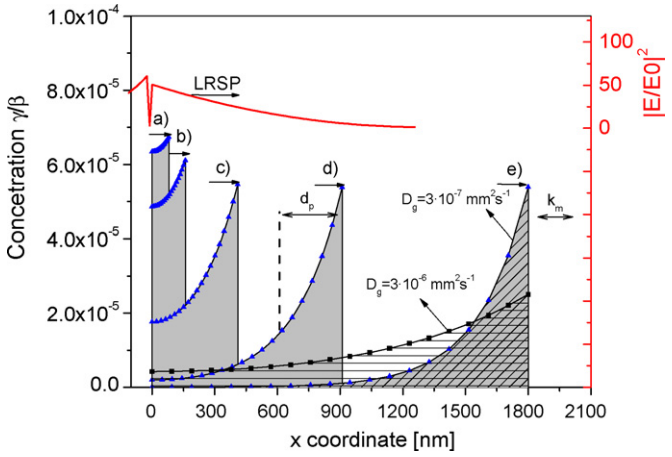

Fig. 5. The comparison of spatial distribution of captured analyte $\gamma(x)$ for the hydrogel thickness of (a) $d_h = 64$ nm, (b) $d_h = 130$ nm, (c) $d_h = 330$ nm, (d) $d_h = 730$ nm and (e) $d_h = 1440$ nm. In these simulations, the $\gamma(x)$ were calculated for the binding of analyte with concentration of $\alpha_0 = 0.67$ pM in a sample for 30 min and diffusion coefficient in the gel of $D_g = 3 \times 10^{-7}$ mm^2 s^{-1} was assumed. In addition, $\gamma(x)$ for diffusion coefficient of $D_g = 3 \times 10^{-6}$ mm^2 s^{-1} (black, ■) and $D_g = 3 \times 10^{-7}$ mm^2 s^{-1} (blue, ▲) is shown for the hydrogel thickness of $d_h = 1800$ nm. The profiles of electric intensity field of LRSP mode are presented for the comparison in the upper part of the graph. (For interpretation of the references to color in this figure legend, the reader is referred to the web version of the article.)

Finally, we discuss the effect of mass transfer of the analyte to the surface that was taken into account using the diffusion rate k_m. When the condition $k_a\beta d_h \gg k_m$ (for large analyte diffusion depth $d_p > d_h$) or $k_a\beta d_p \gg k_m$ (for large hydrogel thickness $d_h > d_p$) holds, the binding of target molecules to the surface is strongly diffusion limited (let us note, that these conditions relates to Damköhler number (Edwards, 2001) that can be expressed as $Da \sim d_{h,p}\beta k_a/k_m$ for the herein studied architecture). This effect is illustrated in Fig. 5 which shows the dependence of the concentration of captured analyte molecules $\gamma(x,t)$ for the hydrogel thickness $d_h = 1440$ nm. When increasing the diffusion coefficient from $D_g = 3 \times 10^{-7}$ to $D_g = 3 \times 10^{-6}$ mm^2 s^{-1}, one can see that the binding of the analyte occurs deeper in the gel but the maximum concentration of $\gamma(x)$ is decreased due to the finite diffusion rate k_m. Therefore, increasing the thickness of the hydrogel d_h or diffusion penetration depth d_p such that surface mass density of catcher molecules within the whole gel $d_h\beta$ or within the analyte diffusion depth $d_p\beta$ is much larger than k_m/k_a will not lead to an enhanced amount of captured analyte and thus will not provide higher sensor response F. For the investigated architecture, the thickness of the hydrogel providing binding capacity that is sufficient for the efficient capture of target analyte diffusing to the sensor surface with the rate $k_m = 2 \times 10^{-3}$ mm s^{-1} is of $k_m/k_a\beta = 345$ nm which is consistent with the experimental data and numerical simulations presented in Fig. 4b.

4. Conclusions

In this work, a high capacity hydrogel binding matrix for evanescent wave affinity biosensors was experimentally and theoretically investigated. The results show that for detection of target analyte with maximum sensitivity, a delicate design of three-dimensional hydrogel binding matrix needs to be carried out. Particularly, the interplay of parameters including the profile of a probing wave, diffusion characteristics of an analyte to and through a gel, binding capacity and affinity rate constants k_a and k_d have to be taken to account. In a model immunoassay experiments, the limit of detection below 20 fM was achieved for optimized hydrogel matrix and long range surface plasmon and hydrogel optical waveguide field-enhanced fluorescence spectroscopy. The presented data indicate that large binding capacity schemes would be particularly beneficial for biosensing with lower-affinity biomolecular recognition

elements or for detection of small molecules that diffuse fast from sample to the sensor surface and through the hydrogel binding matrix. Our future research will include the investigation of binding matrices based on nanostructured hydrogel materials for more efficient capture of target analyte and the exploitation of responsive and molecular imprinted hydrogels.

Acknowledgements

Ulrich Jonas from FORTH/IESL in Heraklion (Greece) and Alena Aulasevich, Basit Yameen and Martina Knecht from the Max Planck Institute for Polymer research in Mainz (Germany) are gratefully acknowledged for the synthesis of NIPAAm polymer and benzophenon-terminated thiol. We also thank to Riccardo Raccis from the Max Planck Institute for Polymer research in Mainz (Germany) for helpful discussions on diffusion of protein molecules in NIPAAm hydrogel. Partial support for this work was provided by the Deutsche Forschungsgemainschaft (KN 224/18-1, Schwerpunktprogramm "Intelligente Hydrogele", SPP 1259) and ZIT, Center of Innovation and Technology of Vienna.

Appendix A. Supplementary data

Supplementary data associated with this article can be found, in the online version, at doi:10.1016/j.bios.2010.07.072.

References

Andersson, O., Larsson, A., Ekblad, T., Liedberg, B., 2009. Biomacromolecules 10, 142–148.
Aulasevich, A., Roskamp, R.F., Jonas, U., Menges, B., Dostalek, J., Knoll, W., 2009. Macromol. Rapid Commun. 30 (9–10), 872–877.
Beines, P.W., Klosterkamp, I., Menges, B., Jonas, U., Knoll, W., 2007. Langmuir 23 (4), 2231–2238.
Brunsen, A., Jonas, U., Dostalek, J., Menges, B., Knoll, W., in preparation.
Edwards, D.A., 2001. Bull. Math. Biol. 63, 301–327.
Hale, G.M., Querry, M.R., 1973. Appl. Optics 12 (3), 555–563.
Homola, J., 2008. Chem. Rev. 108, 462–493.
Huang, C.J., Dostalek, J., Knoll, W., 2010. J. Vacuum Sci. Technol. B 28 (1), 66–72.
Huang, C.J., Jonas, U., Dostalek, J., Knoll, W., 2009. Proc. SPIE 7356, 735625.
Jossang, T., Feder, J., Rosenqvist, E., 1988. J. Protein Chem. 7 (2), 1573–4943.
Lofas, S., Johnsson, B., 1990. J. Chem. Soc., Chem. Commun. 21, 1526–1528.
Masson, J.F., Battaglia, T.M., Kim, Y.C., Prakash, A., Beaudoin, S., Booksh, K.S., 2004. Talanta 64, 716–725.
Perlmann, G.E., Longsworth, L.G., 1948. J. Am. Chem. Soc. 70 (8), 2719–2724.
Raccis, R., personal communication.
Schuck, P., 1996. Biophys. J. 70 (3), 1230–1249.
Sikavitsas, V., Nitsche, J.M., Mountziaris, T.J., 2002. Biotechnol. Prog. 18, 885–897.
Tanaka, H., Hanasaki, M., Isojima, T., Takeuchi, H., Shiroya, T., Kawaguchi, H., 2009. Colloids Surfaces B 70, 259–265.
Vasilev, K., Knoll, W., Kreiter, M., 2004. J. Chem. Phys. 120 (7), 3439–3445.
Voellenkle, C., Weigert, S., Ilk, N., Egelseer, E., Weber, V., Loth, F., Falkenhagen, D., Sleytr, U.B., Sara, M., 2004. Appl. Environ. Microbiol. 70 (3), 1514–1521.
Wang, Y., Brunsen, A., Jonas, U., Dostalek, J., Knoll, W., 2009a. Anal. Chem. 81 (23), 9625–9632.
Wang, Y., Dostalek, J., Knoll, W., 2009b. Biosens. Bioelectron. 24 (7), 2264–2267.
Wang, Y., Jonas, U., Wei, T., Dostalek, J., Knoll, W., 2010. Biosens. Bioelectron. 25, 1663–1668.
Yeh, P., 1998. Optical Waves in Layered Media. John Wiley and Sons, New York.
Yu, F., Persson, B., Lofas, S., Knoll, W., 2004. Anal. Chem. 76 (22), 6765–6770.